



| | |
|------------------|---|
| Title | Corrosion resistant TiO ₂ film formed on magnesium by liquid phase deposition treatment |
| Author(s) | Fujita, R.; Sakairi, M.; Kikuchi, T.; Nagata, S. |
| Citation | Electrochimica Acta, 56(20), 7180-7188 https://doi.org/10.1016/j.electacta.2011.03.146 |
| Issue Date | 2011-08-01 |
| Doc URL | http://hdl.handle.net/2115/47210 |
| Type | article (author version) |
| File Information | EA56-20_7180-7188.pdf |



[Instructions for use](#)

Corrosion resistant TiO₂ film formed on magnesium by liquid phase deposition treatment

R. Fujita¹⁾, M. Sakairi²⁾, T. Kikuchi²⁾ and S. Nagata³⁾

¹⁾ Research Group of Materials Design, Division of Materials Science and Engineering,
Graduate School of Engineering, Hokkaido University, Kita-13, Nishi-8, Kita-ku, Sapporo,
060-8628, Japan

²⁾ Research Group of Materials Design, Division of Materials Science and Engineering,
Faculty of Engineering, Hokkaido University, Kita-13, Nishi-8, Kita-ku, Sapporo, 060-8628,
Japan

³⁾ Institute for Materials Research, Tohoku University, Katahira-2-1-1, Aoba-ku, Sendai,
980-8577, Japan

Abstract

Liquid phase deposition treatment (LPD) was applied to form a corrosion protective titanium dioxide (TiO_2) film on commercially available pure magnesium. Changing the solution pH, from acidic to highly alkaline, and with the addition of sucrose, it becomes possible to form a highly adhesive and thin TiO_2 film on commercially available pure magnesium without any heat treatment. The role of the sucrose may be attributed to the formation of tetrafluoroboric acid (BF_4^-) in the solution reducing the homogeneous nucleation of TiO_2 in the LPD solution. The film formed in the weak alkaline environment shows better corrosion resistance than at other LPD conditions, while the average rest potential is the same as that of as-polished specimens. This low rest potential may be due to micro-cracks in the formed film and high activity of the magnesium substrate.

Keywords: Magnesium; Corrosion behavior; Liquid phase deposition

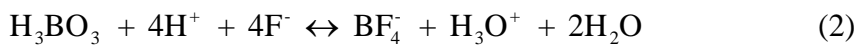
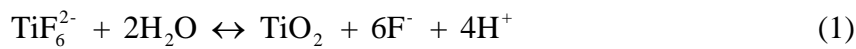
1. Introduction

Because global warming has recently attracted much attention, environmental consciousness has become higher worldwide, and increasing amounts of carbon dioxide (CO₂) in the air is one possible reason for the recent global warming. Large volumes of CO₂ are emitted by transport systems such as automobiles and airplanes, and reducing CO₂ emissions from transport systems is urgently required. Reducing the weight of vehicles etc. by using high strength to weight ratio compounds is an effective way to reduce CO₂ emissions.

Magnesium and its alloys are candidates for reducing the weight of automobiles and airplanes, but magnesium-based components have very low corrosion resistance in many environments [1-3]. Solving the corrosion problem is a key element to enable wider use of magnesium-based components. Therefore, much research has tried to increase corrosion resistance by surface treatments. Okido et al. and Wu et al. reported the fabrication of corrosion resistant magnesium oxide (MgO) films on magnesium by anodizing [4, 5]. Campo et al. and Arrabal et al. reported formation of coated corrosion resistant silicon carbide (SiC) films on magnesium by thermal sprays [6, 7]. Truong et al. and Kannan et al. reported corrosion resistant polymer films on magnesium [8, 9]. The corrosion problem of magnesium

still remains however, and an effective coating for corrosion protection is still needed.

Liquid phase deposition treatment (LPD) is a new surface coating technique, which can form metal oxide film by dipping the substrate in aqueous solutions [10]. This technique can be applied to form metal oxide films on many kinds of substrate. Deki et al. reported fabrication of TiO₂ nanostructures on silicon wafers with LPD and electron lithography [11]. Lee et al. reported fabrication of photo catalytic TiO₂ films on stainless steel [12]. The present study attempts to form TiO₂ film on magnesium substrate. The possible chemical reactions are as follows [11, 12].



Equation (1) is the main reaction forming TiO₂ film, and it scavenges the F⁻ and H⁺ ions with (equation (2)), where boric acid (H₃BO₃) is added in the solutions. When magnesium is dipped in F⁻ ion containing solutions, magnesium fluoride (MgF₂) will form on the surface and reduce further magnesium dissolution [13]. Therefore, LPD can be applied in this manner to form TiO₂ film as a surface treatment to increase the corrosion resistance of magnesium.

Hu et al. reported the fabrication of corrosion resistant TiO₂ film on a magnesium alloy, AZ31,

by LPD with an annealing treatment [14]. They reported that with increases in the annealing temperature and at longer annealing times, the corrosion resistance of AZ31 was improved. However, the annealing treatment reduces the advantages of LPD to form oxide films simply on substrates. Therefore, when LPD is applied industrially to form protective oxide films on magnesium and its alloys, a process not involving annealing would be advantageous.

It is well known that magnesium is stable in alkaline solutions [15]. In alkaline (high pH) solutions, magnesium substrate will not dissolve during LPD treatment, and TiO_2 deposition on magnesium substrate may be more stable than LPD treatment in acidic (low pH) solutions. However, there is no research reporting LPD with alkaline solutions on magnesium substrate.

Commonly, magnesium alloys such as AZ31 or AZ91 are used, but alloying elements may make it difficult to elucidate the formation kinetics and film structure with these alloys. Here, commercially available pure magnesium was used as the specimens. The purpose of this study is to investigate optimum LPD conditions without heat treatment for corrosion resistant TiO_2 film formation and to investigate the corrosion resistance properties of the formed TiO_2 films by immersion and electrochemical corrosion tests.

2. Experimental

2.1 Specimens

Magnesium sheet (99 mass%, 25 mm×15 mm×3 mm) was used as specimens, before the LPD, specimens were mechanical ground by grinding machine (Struers Inc., A/S S5629) and SiC paper (#600, #1000 and #1500). Ground specimens were ultrasonically cleaned in ethanol (Kanto Chemical Co. Ltd., 99.5 mass%) for 600 s.

2.2 Liquid phase deposition (LPD)

Specimens were immersed in 0.01 kmol m⁻³ ammonium hexafluorotitanate ((NH₄)₂TiF₆) (Sigma Aldrich Inc., 99.99 mass%) / 0.02 kmol m⁻³ H₃BO₃ (Kanto Chemical Co. Ltd., 99.5 mass%) with or without 0.2 kmol m⁻³ sucrose (Kanto Chemical Co. Ltd., guaranteed reagent) up to 86.4 ks at 353 K. The pH of the solutions was adjusted with sodium hydroxide (NaOH) (Kanto Chemical Co. Ltd., 97.0 mass%) and an acidic solution (Acid: pH = 3.5), a low alkaline solution (L-base: pH = 9.5), and a high alkaline solution (H-base: pH = 13.5) were prepared. Sucrose acts an inhibitor for TiO₂ excess homogeneous nucleation in alkaline LPD solutions of L- and H-base specimens. The effect of the sucrose on the nucleation was

evaluated by the change in appearance of the LPD solutions.

2.3 Corrosion tests

Corrosion tests were carried out in 0.3 dm³ glass separable flasks. Specimens, as prepared and subjected to LPD were immersed in 0.53 kmol m⁻³ (about 3 mass%) sodium chloride (NaCl) (Kanto Chemical Co. Ltd., 99.5 mass%) solution at 298 K for 86.4 ks. The rest potential of the specimens during the immersion corrosion tests were measured by potentiostat (Toho Technical Research Co. Ltd., PS-14). An Ag/AgCl/sat. KCl electrode was used as the reference electrode. Potentiodynamic polarization tests were carried out in 0.53 kmol m⁻³ NaCl solution at 298 K from -1.70 V to -1.45 V (potential sweep rate 1 mV s⁻¹) using a potentiostat (Toho Technical Research Co. Ltd., PS-14) and a function generator (Hokuto Denko Corporation, HB-305). These tests were carried out directly after the specimens had been immersed in the test solutions. An Ag/AgCl/sat. KCl electrode was used as the reference electrode and a Pt electrode was used as the counter electrode.

2.4 Characterization of the deposited films

Specimen surfaces before and after the tests were examined by a scanning electron microscope (SEM, Hitachi High-Technologies Co., TM-1000 and JEOL Ltd., JSM-6510LA) and an optical microscope (OM, Wraymer Inc., SW-700TD). The cross sections of the LPD specimens were examined by a transmission electron microscope (TEM, JEOL Ltd., JEM-2000FX) equipped with an energy dispersive X-ray spectroscope (EDS). The oxide films were also analyzed by an X-ray photoelectron spectroscope (XPS, JEOL Ltd., JPS-9200) using an Mg K α X-ray source (1253.6 eV), and Rutherford Backscattering Spectroscopy (RBS, High Voltage Engineering Tandetron) used a 2.0 MeV He²⁺ ion beam supplied by a Van de Graff accelerator. The He²⁺ ion beam angle was normal to the specimen surface, and the detector angle was 170 degrees to the incident direction. The chemical composition and thickness of the formed films were determined using the RUMP program. The adhesion of the formed film was examined by scotch tape peeling tests. The scotch tape was adhered to the specimens at 5.0×10^4 N m⁻² and peeled off vertical to the specimen. The surfaces before and after the adhesion tests were observed by SEM.

3. Results

3.1 Effect of pH and sucrose on LPD solution appearance

Fig. 1 shows the changes in appearance of the LPD solutions of Acid, L-base, and H-base solutions with and without sucrose at 3.6 ks, 353 K. The Acid solution shows little difference, with and without sucrose both are white opaque solutions with the white turbidity caused by TiO_2 particles formed by homogeneous nucleation in the LPD solutions [12]. The L-base and H-base solutions show an apparent difference in the TiO_2 nucleation rate by the addition of sucrose. The L-base and H-base solutions without sucrose are white (opaque), while the L-base and H-base solutions with sucrose are transparent.

It is critically important to inhibit excess nucleation of TiO_2 to be able to form a protective TiO_2 film on the magnesium substrate. Therefore, the Acid (without sucrose), L-base (with sucrose), and H-base (with sucrose) conditions were selected as the LPD conditions in the following experiments.

Fig. 2 shows the changes in appearance of the LPD solutions of Acid, L-base, and H-base with elapsed time. The LPD solutions were maintained at 353 K in an oil bath. White deposits were seen in the H-base solution at 7.2 ks. Similar deposits were observed in the L-base condition at 43.2 ks, however, here the nucleation rate of TiO_2 is slower than in the H-base

condition. In the Acid condition, the solution changes to a white opaque liquid at 7.2 ks. This result suggests that the nucleation rate of TiO_2 in the Acid condition is the most rapid among these three conditions.

The change of TiO_2 film coverage of magnesium substrate with LPD duration was also examined in all the solutions. In the shorter period (< 86.4 ks) LPD treatments, magnesium substrate showed little coverage by TiO_2 film in all solutions. Therefore the LPD treatment duration of 86.4 ks is investigated in the following experiments.

3.2 Characterization of LPD specimens

Fig. 3 shows surface images of as-polished (only ground by SiC paper) and LPD specimens by OM and SEM. The Acid surface appears white from the OM image, and it is covered by powder-like substances, which were nucleated in the solution, as observed by the SEM image. These particles were anatase-type TiO_2 as examined by Raman spectroscopy [16]. The L-base specimen surface does not show large differences from the as-polished specimen, as observed by the OM image, however scratches formed by the grinding and appearing in the SEM image became indistinct. This result suggests that the surface of the specimen is covered with

a relatively thick oxide film. The surface morphology of the H-base specimens appears very similar to the as-polished specimens.

Fig. 4 shows XPS spectra of the LPD specimens. In the Ti 2p spectra, there are two peaks (464.5 eV and 459.0 eV) in the Acid and L-base specimens originating from Ti 2p_{1/2} and Ti 2p_{3/2} of TiO₂ [17-20]. Only one peak (459.0 eV) is observed in the H-base specimen, indicating that H-base specimens also have a TiO₂ layer. In O 1s, the Acid specimen has a peak at 529.8 eV, while the L-base specimen has two peaks at 529.8 eV and 532.9 eV, here the H-base specimen has a peak at 532.9 eV. The peak at 529.8 eV corresponds to O²⁻ and the peak at 532.9 eV corresponds to OH⁻ [17, 20, 21]. In the Mg 2p spectra, a peak at 50.2 eV is observed in the L-base and H-base specimens. This peak corresponds to Mg²⁺ [18]. In the F 1s spectra, all specimens have a peak at 685.6 eV. This peak corresponds to F⁻ [18]. From these XPS spectra, the Acid specimen surface can be considered to be covered by TiO₂ and F⁻ in the LPD solution adsorbs onto the surface of TiO₂ [22]. The L-base specimen surface is considered to be formed by TiO₂, MgF₂ and Mg(OH)₂, and the F⁻ may have adsorbed onto the surface. The H-base specimen surface is considered to be formed by TiO₂ and Mg(OH)₂. There may also be MgF₂ and adsorbed F⁻ on the H-base specimen surface.

Fig. 5 shows cross sectional TEM images of the LPD specimens. The film thicknesses of the Acid, L-base, and H-base specimens are approximately 582 nm, 618 nm, and 363 nm, respectively. The results of the chemical composition analyses of the formed films by TEM-EDS (spot 1 to spot 6) are shown in Table 1. From the results of Spot 1 and 2, the film formed in the Acid condition contains O, F, and Mg both in the outer layer and in the inner layer. Magnesium easily forms an MgF_2 layer in solutions that contain F^- and $\text{Mg}(\text{OH})_2$ is formed in the presence of H_2O [14]. The O and F observed by TEM-EDS may derive from $\text{Mg}(\text{OH})_2$ and MgF_2 formed by the LPD, considering that the Acid specimen has an $\text{Mg}(\text{OH})_2$ / MgF_2 layer. The amount of Ti observed by the TEM-EDS analysis is small. This is because powder-like TiO_2 on the surface, which was observed by SEM, peeled off during the TEM sample preparation. The RBS result showed that the thickness of the powder-like TiO_2 layer was more than 2 μm . From the results of Spots 3, 4, and the XPS spectra, the outer layer of the L-base specimen contains TiO_2 and $\text{Mg}(\text{OH})_2$ and the inner layer contains MgF_2 and $\text{Mg}(\text{OH})_2$. The inner layers contain excess oxygen according to the TEM-EDS analysis results in Table 1. This may be due to adsorbed H_2O . From the results of Spot 5, 6, and the XPS spectra the film on the H-base specimen contains $\text{Mg}(\text{OH})_2$ and TiO_2 is present on the surface.

The thickness of the TiO_2 layer was thinner than that on the L-base specimen examined by RBS. The film on the H-base specimen also has an excess of Mg in the inner layer as examined by TEM-EDS. This is likely due to the signal of the magnesium substrate rather than any Mg in the surface film.

Fig. 6 shows SEM images of the surfaces before and after the peeling tests by scotch tape (details in section 2.4). The tests were carried out three times and the surfaces were observed at the same area after each test. The Acid specimen shows large changes after the 1st peeling test, almost all of the film appears to have been peeled off. After the 2nd and 3rd peeling tests, the surface morphology does not change further. The H-base specimen shows limited changes after the 1st peeling test and very limited changes after the 2nd and 3rd peeling tests. The L-base specimen shows almost no change resulting from the peeling tests, showing that films formed in the L-base condition have the better adhesion among these three LPD conditions.

Fig. 7 shows XPS spectra for the Acid and L-base specimens after the 3rd peeling test. The Acid specimen shows Ti 2p and F 1s peaks, and Mg 2p. The O 1s peak is at 529.8 eV, different from the 532.9 eV position in Fig. 4. These results suggest that the formed TiO_2 and $\text{Mg}(\text{OH})_2$ / MgF_2 layer were peeled off by the peeling tests, and that magnesium substrate

newly exposed has formed new $\text{Mg}(\text{OH})_2$ by the H_2O and O_2 in the atmosphere. This result is in good agreement with the surface morphology changes shown in Fig. 6. The L-base spectra show little or no change in the peaks of Ti 2p and O 1s by the peeling tests. These XPS results suggest that the film of the L-base specimen has good adhesiveness.

From the SEM, TEM-EDS, and XPS results, the condition of the L-base specimen makes it suitable to form corrosion resistant TiO_2 films on magnesium by LPD.

3.3 Corrosion tests

Polarization curves of the as-polished and the LPD specimens are shown in Fig. 8. All LPD specimens display anodic and cathodic currents that are smaller than those of the as-polished specimen. The L-base specimens show the lowest anodic current among these specimens, while the cathodic current of L-base is the largest among the LPD specimens. It is not clear why the cathodic current of the L-base specimen is the largest, but one possibility is that the highly adhesive and homogeneous TiO_2 film on this specimen acts as an n-type semiconductor. The unclear Tafel region in the measured polarization curves makes it difficult to discuss the corrosion current and corrosion potential further. From the order of the anodic

currents, the L-base specimen would show the higher corrosion resistance among these specimens. To elucidate further details of the polarization behavior of the LPD specimens, further experiments are required.

Fig. 9 shows changes in the rest potential of the as-polished and LPD specimens during the immersion corrosion test. All specimens show rest potentials of approximately -1.6 V, and the Acid and as-polished specimens show large potential fluctuations. These potential fluctuations are related to localized corrosion of the specimen and formation of corrosion products [23-27]. When corrosion products cover the surface, they inhibit further corrosion of the specimen and cause a shift towards more positive potentials and the removal of the corrosion products in turn causes a negative shift in the potentials.

Fig. 10 shows surface images of as-polished and LPD specimens after immersion corrosion tests for 86.4 ks by OM and SEM. The as-polished specimen surface changes to become very irregular, and the Acid specimen in the OM and SEM images shows localized corrosion. Only a few cracks, which may have formed as a result of the immersion corrosion tests, are observed on the SEM image of the L-Base specimen surface. The H-base specimen is also corroded like the as-polished specimen. These corrosion test results indicate that the oxide film formed in L-base has good corrosion resistance in spite of the low rest potential during the immersion corrosion test.

4. Discussion

4.1 Effect of sucrose on film formation

It is important to inhibit excess homogeneous nucleation of TiO_2 in LPD solutions to promote the formation of TiO_2 film on the magnesium substrate by heterogeneous nucleation, and sucrose has been shown to affect this (see section 3.1). Fig. 11 shows a schematic representation of the role of sucrose in the LPD solution. The H_3BO_3 is decomposed into B^{3+} by H^+ in the LPD solution and then B^{3+} causes the formation of tetrafluoroboric acid (BF_4^-) by F. The nucleation of TiO_2 is preceded by B^{3+} in the LPD solution (equations (1) and (2)), and in the presence of sucrose, some B^{3+} may form complexes with the sugar group of sucrose to release H^+ from the sugar group [28]. The reaction does not appear to take place in low pH solutions (Acid), because the appearance of the solution of Acid samples shows little or no difference with and without sucrose in Fig. 1.

4.2 LPD conditions and formed films

The pH and sucrose are very affective to change the formed oxide film composition and

structure. Fig. 12 shows a schematic illustration of the film generating processes in different LPD conditions.

From the SEM, XPS, and TEM-EDS results, the Acid specimen surfaces have a double layer structure, inner $\text{Mg(OH)}_2 / \text{MgF}_2$ and outer powder-like TiO_2 . An $\text{Mg(OH)}_2 / \text{MgF}_2$ layer was initially formed in the Acid condition and then the accumulated TiO_2 particles, which were formed in the solution like in Fig. 1, were deposited on the $\text{Mg(OH)}_2 / \text{MgF}_2$ layer.

From the XPS and TEM-EDS results, the L-base specimen surface has a double layer structure, inner $\text{Mg(OH)}_2 / \text{MgF}_2$ layer, and outer $\text{Mg(OH)}_2 / \text{TiO}_2$ layer. Because the L-base solution pH is 9.5, the Mg(OH)_2 phase is stable here [15]. From this, it may be surmised that the Mg(OH)_2 film was formed at the initial stage of the LPD, however the formed Mg(OH)_2 film may have defects, then H_2O and F^- ions in the solution can reach the magnesium substrate and form an $\text{Mg(OH)}_2 / \text{MgF}_2$ layer under the Mg(OH)_2 layer. An $\text{Mg(OH)}_2 / \text{TiO}_2$ layer was also formed from the initial stage of the LPD immersion, however, the deposition rate of the TiO_2 is very slow and TiO_2 is observed only at the outer layer of the formed film.

In H-Base, an Mg(OH)_2 layer was formed and a very thin $\text{Mg(OH)}_2 / \text{TiO}_2$ layer was

formed on the $\text{Mg}(\text{OH})_2$ layer, because homogeneous nucleation of TiO_2 is predominant and the concentration of TiF_6^{2-} in this solution decreased as shown in Fig. 1.

4.3 Corrosion behavior of LPD treated specimens

The corrosion resistances of the different LPD specimens were different. Acid specimens show localized corrosion and here the powder-like TiO_2 on the surface shown in Fig. 3 may inhibit the intrusion of NaCl solution into the $\text{Mg}(\text{OH})_2 / \text{MgF}_2$ layer at the initial stage. This powder-like TiO_2 is easily peeled off as shown in Fig. 6. When the TiO_2 particles peel off and expose the $\text{Mg}(\text{OH})_2 / \text{MgF}_2$ layer to the NaCl solution, the magnesium substrate is rapidly corroded because $\text{Mg}(\text{OH})_2$ and MgF_2 are not stable in the presence of Cl^- in the solutions [14].

The L-base specimens showed high corrosion resistance due to the presence of the adhesive $\text{Mg}(\text{OH})_2 / \text{TiO}_2$ layer on the magnesium surface as shown in Fig. 6 and Fig. 7. However, the rest potential during the immersion corrosion test showed low potentials, between -1.6 V and -1.5 V. The film may contain micro-cracks and such micro-cracks would enable the NaCl solution to reach and corrode the magnesium substrate [29].

The H-base specimens were heavily corroded, like the as-polished specimens, indicating that at high pH the LPD solution did not form a protective oxide film on the magnesium. The XPS and TEM-EDS analyses showed the presence of TiO_2 , however, this TiO_2 layer was not sufficient to prevent corrosion of the magnesium substrate. The formed $\text{Mg}(\text{OH})_2 / \text{TiO}_2$ film does not protect the magnesium substrate in the presence of Cl^- in the solutions.

5. Conclusions

This is a report of LPD (liquid phase deposition treatment) applied to form corrosion resistant TiO_2 film on commercially available pure magnesium and it also investigates the effect of LPD conditions on film structure and corrosion resistance. The following conclusions may be drawn.

1. The formed films are double layer structures of an inner $\text{Mg}(\text{OH})_2 / \text{MgF}_2$ layer and an outer powder-like TiO_2 layer when formed at $\text{pH} = 3.5$ (Acid condition); a double layer structure of an inner $\text{Mg}(\text{OH})_2 / \text{MgF}_2$ layer and an outer $\text{Mg}(\text{OH})_2 / \text{TiO}_2$ layer when formed at $\text{pH} = 9.5$ (L-base condition); and a double layer structure of an inner $\text{Mg}(\text{OH})_2$ layer and an

outer $\text{Mg}(\text{OH})_2 / \text{TiO}_2$ layer when formed at $\text{pH} = 13.5$ (H-base condition).

2. The addition of sucrose to the LPD solutions makes it possible to reduce excess homogeneous nucleation of TiO_2 and increase heterogeneous nucleation on the magnesium substrate.

3. The film formed in the L-base condition shows better corrosion resistance than the films formed at other LPD conditions, while the average rest potential of the resulting specimens is the same as the as-polished specimens. This low rest potential may be due to micro-cracks in the film and the high activity of the magnesium substrate.

References

- [1] A. Pardo, M. C. Merino, A. E. Coy, R. Arrabal, F. Viejo and E. Matykina, *Corros. Sci.* 50 (2008) 823.
- [2] R. Lindstrom, L. G. Johansson, G. E. Thompson, P. Skeldon and J. Svensson, *Corros. Sci.* 46 (2004) 1141.
- [3] R. Ambat, N. N. Aung and W. Zhou, *J. Appl. Electrochem.* 30 (2000) 865.
- [4] L. Chai, X. Yu, Z. Yang, Y. Wang and M. Okido, *Corros. Sci.* 50 (2008) 3274.
- [5] C. S. Wu, Z. Zhang, F. H. Cao, L. J. Zhang, J. Q. Zhang and C. N. Cao, *Appl. Surf. Sci.* 253 (2007) 3893.
- [6] M. Campo, M. Carboneras, M. D. Lopez, B. Torres, P. Rodrigo, E. Otero and J. Rams, *Surf. Coat. Tech.* 203 (2009) 3224.
- [7] R. Arrabal, A. Pardo, M. C. Merino, M. Mohedano, P. Casajus and S. Merino, *Surf. Coat. Tech.* 204 (2010) 2767.
- [8] V. T. Truong, P. K. Lai, B. T. Moore, R. F. Muscat and M. S. Russo, *Synthetic Met.* 110 (2000) 7.
- [9] M. B. Kannan, D. Gomes, W. Dietzel and V. Abetz, *Surf. Coat. Tech.* 202 (2008) 4598.

- [10] S. Deki, Y. Aoi, O. Hiroi and A. Kajinami, *Chem. Lett.* 25 (1996) 433.
- [11] S. Deki, S. Iizuka, A. Horie, M. Mizuhata and A. Kajinami, *Chem. Mater.* 16 (2004) 1747.
- [12] S. C. Lee, H. Yu, J. Yu and C.H. Ao, *J. Cryst. Growth* 295 (2006) 60.
- [13] G. Song and A. Atrens, *Adv. Eng. Mater.* 5 (2003) 837.
- [14] J. Hu, G. Shaokang, C. Zhang, C. Ren, C. Wen, Z. Zeng and L. Peng, *Surf. Coat. Tech.* 203 (2009) 2017.
- [15] G. G. Perrault, *Electroanal. Chem. Interfacial Electrochem.* 51 (1974) 107.
- [16] M. Sakairi, R. Fujita, T. Kikuchi and S. Nagata, *Proc. of 5th International Symposium on Marine Corrosion and Control* (2011) 277.
- [17] A. O. T. Patrocínio, E. B. Paniago, R. M. Paniago and N. Y. M. Iha, *Appl. Surf. Sci.* 254 (2008) 1874.
- [18] S. H. Woo and C. K. Hwangbo, *Surf. Coat. Tech.* 201 (2007) 8250.
- [19] J. Liang, L. Hu and J. Hao, *Electrochim. Acta* 52 (2007) 4836.
- [20] Y. L. Wang, *Surf. Coat. Tech.* 150 (2002) 257.
- [21] H. B. Yao, Y. Li and A. T. S. Wee, *Appl. Surf. Sci.* 158 (2000) 112.

- [22] H. Y. Y. Ko, M. Mizuhata, A. Kajinami and S. Deki, *J. Fluor. Chem.* 120 (2003) 157.
- [23] A. M. Lafront, W. Zhang, S. Jin, R. Tremblay, D. Dube and E. Ghali, *Electrochim. Acta* 51 (2005) 489.
- [24] K. Otani, M. Sakairi, T. Kikuchi and A. Kaneko, *Zairyo-to-Kankyo* 59 (2010) 330.
- [25] G. Nakayama, *Zairyo-to-Kankyo* 52 (2003) 477.
- [26] L. Wang, T. Shinohara and B. P. Zhang, *J. Solid State Electrochem.* 14 (2010) 1897.
- [27] L. Wang, B. P. Zhang and T. Shinohara, *Mater. Des.* 31 (2010) 857.
- [28] M. J. Karpa, P. J. Duggan, G. J. Griffin and S. J. Freudigmann, *Tetrahedron* 53 (1997) 3669.
- [29] H. Altun and S. Sen, *Surf. Coat. Tech.* 197 (2005) 193.

Caption list:

Table 1 EDS analysis results of spots 1 to 6 in Fig. 5 (at. %).

Fig. 1 Appearance of the LPD solutions with and without sucrose at 3.6 ks, 353 K..

Fig. 2 Appearance of the LPD solutions at different elapsed times at 353 K.

Fig. 3 Surface images of as-polished and LPD treated specimens by OM and SEM.

Fig. 4 Surface XPS spectra of LPD treated specimens.

Fig. 5 TEM images of cross sections of LPD treated specimens.

Fig. 6 SEM images of surfaces before and after the scotch tape peeling tests.

Fig. 7 Surface XPS spectra of Acid and L-base specimens after the 3rd peeling test.

Fig. 8 Polarization curves of the as-polished and LPD treated specimens.

Fig. 9 Changes in the rest potential of the LPD treated specimens during immersion corrosion tests.

Fig. 10 Surface images of as-polished and LPD treated specimens after immersion corrosion tests for 86.4 ks by OM and SEM.

Fig. 11 Schematic representation of the role of sucrose in the LPD solution.

Fig. 12 Schematic illustrations of the film fabricating processes at different LPD conditions (a) Acid condition, (b) L-base condition and (c) H-base condition.

| | Spot 1 | Spot 2 | Spot 3 | Spot 4 | Spot 5 | Spot 6 |
|-----------|---------------|---------------|---------------|---------------|---------------|---------------|
| Ti | 0.10 | 0.09 | 21.59 | 0.00 | 0.99 | 0.00 |
| O | 28.11 | 34.76 | 62.53 | 30.43 | 69.86 | 49.71 |
| Mg | 60.75 | 50.64 | 15.88 | 52.50 | 29.15 | 50.29 |
| F | 11.04 | 14.51 | 0.00 | 17.10 | 0.00 | 0.00 |

Table 1
R. Fujita et al.

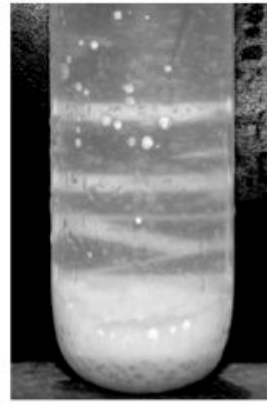
| | without sucrose | with sucrose |
|-------------------------------|---|--|
| Acid (pH = 3.5) |  |  |
| L-base (pH = 9.5) |  |  |
| H-base (pH = 13.5) |  |  |

Fig. 1
R. Fujita et al.

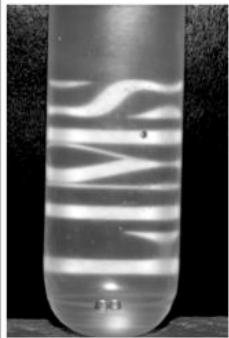
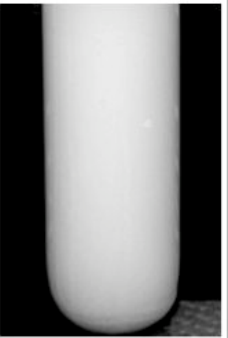
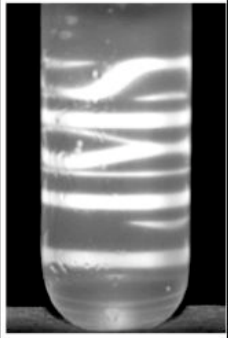
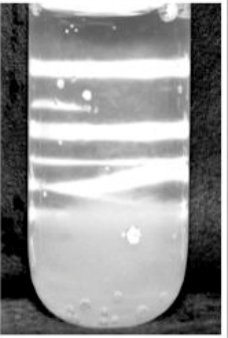
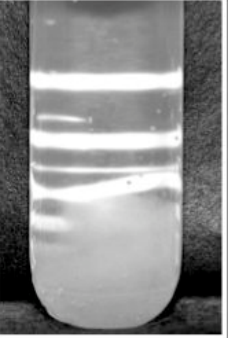
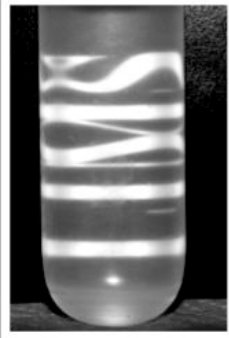
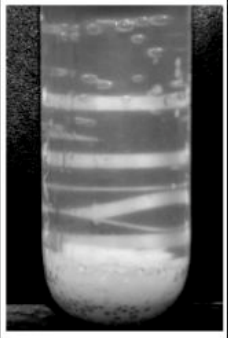
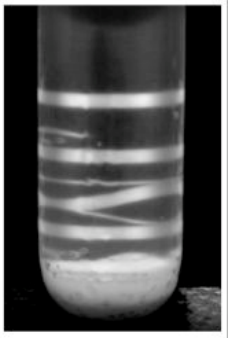
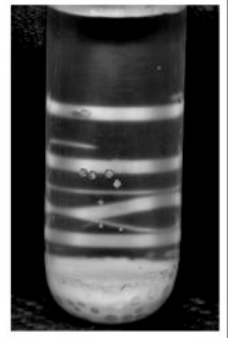
| Time (ks) | 0 (before heating) | 7.2 | 43.2 | 86.4 |
|---------------|---|---|--|---|
| Acid |  |  |  |  |
| L-base |  |  |  |  |
| H-base |  |  |  |  |

Fig. 2
R. Fujita et al.

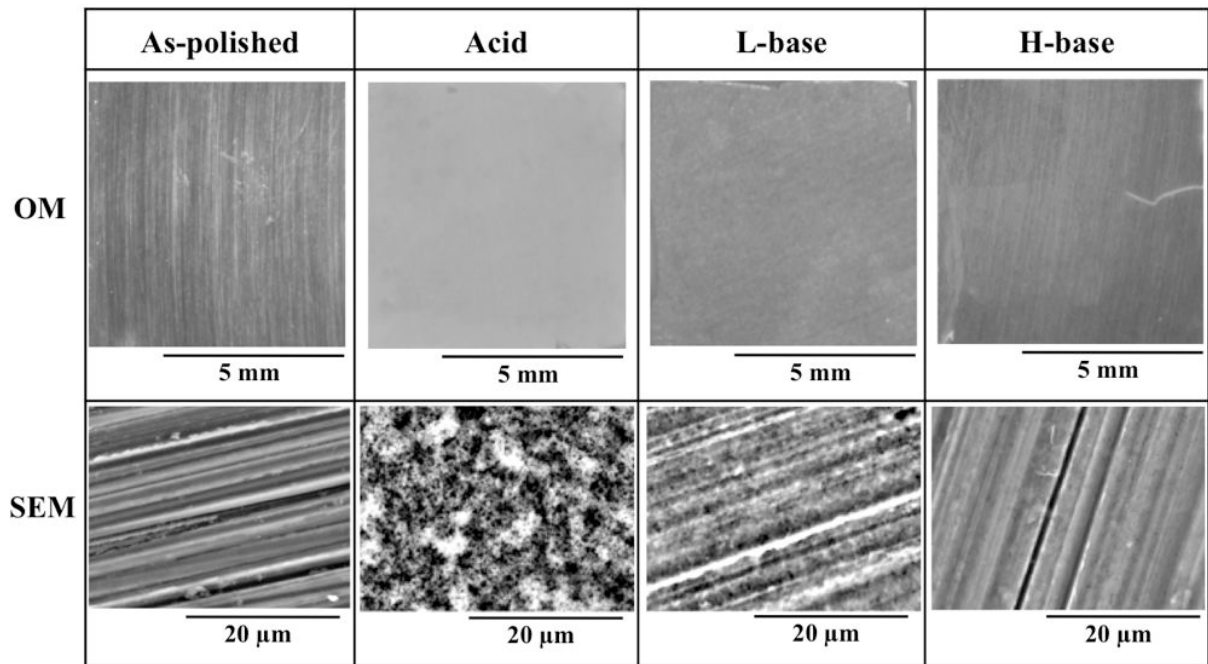


Fig. 3
R. Fujita et al.

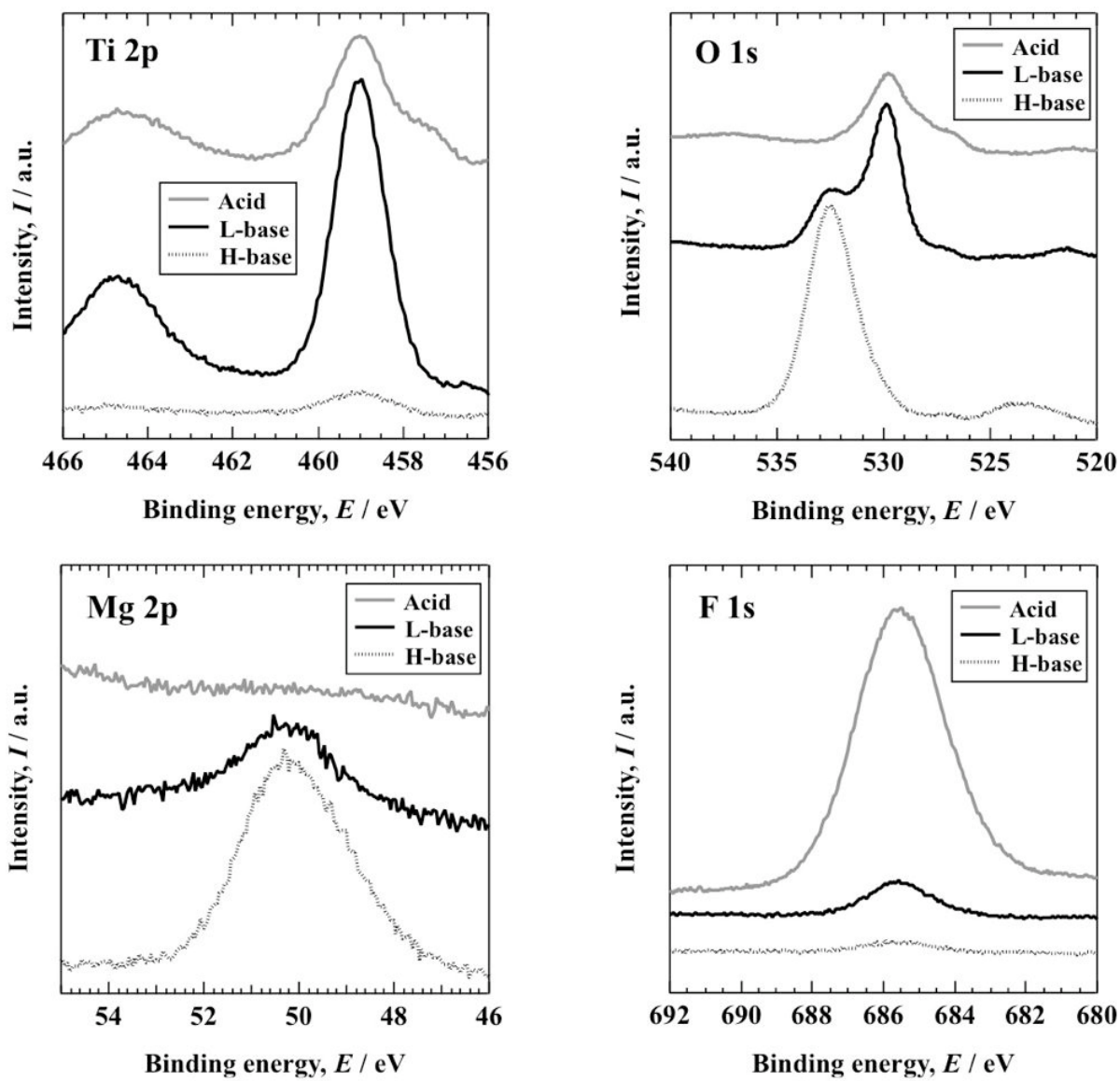


Fig. 4
R. Fujita et al.

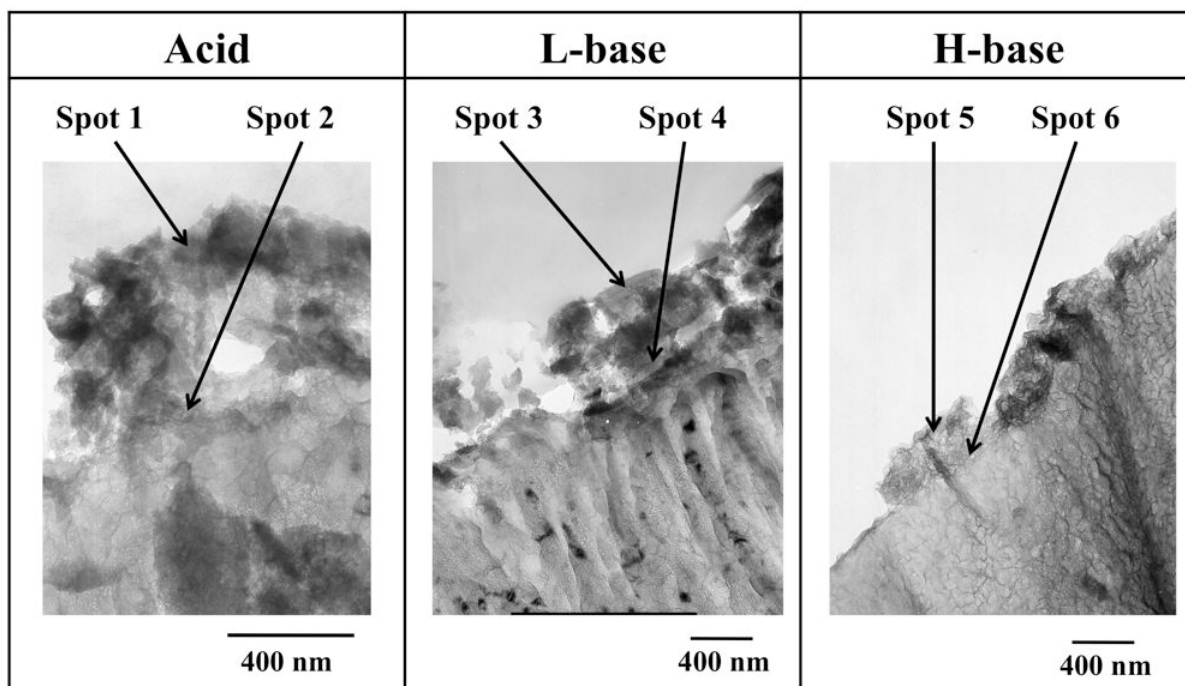
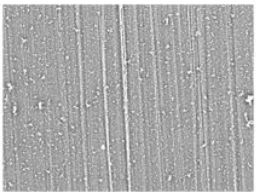
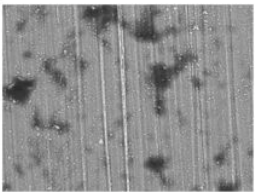
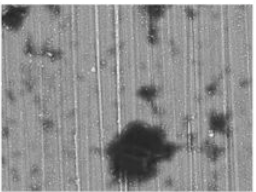
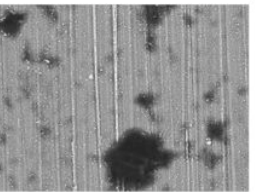
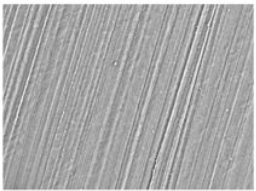
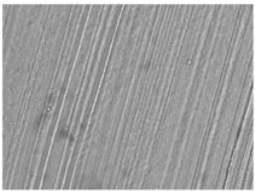
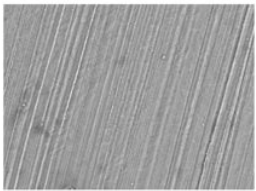
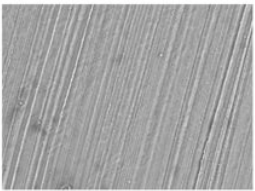
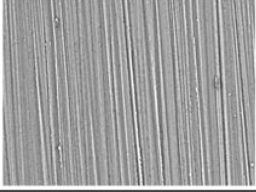
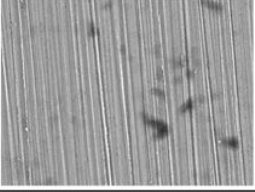
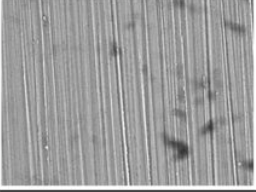
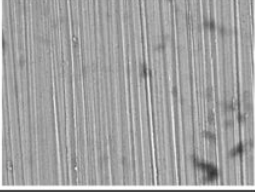


Fig. 5
R. Fujita et al.

| | Before peeling test | After 1st peeling test | After 2nd peeling test | After 3rd peeling test |
|--------|---|---|--|---|
| Acid |  |  |  |  |
| L-base |  |  |  |  |
| H-base |  |  |  |  |

100 μm

Fig. 6
R. Fujita et al.

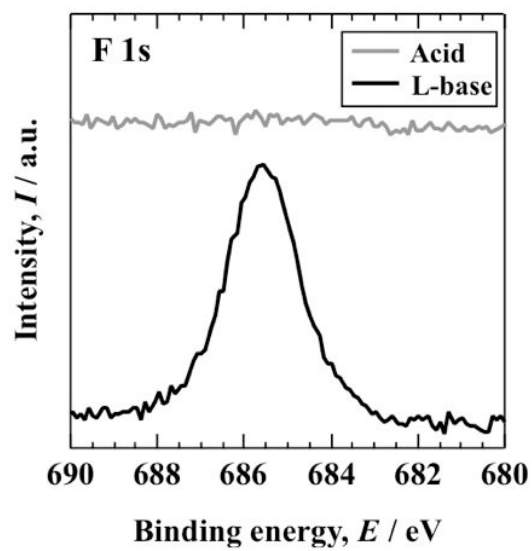
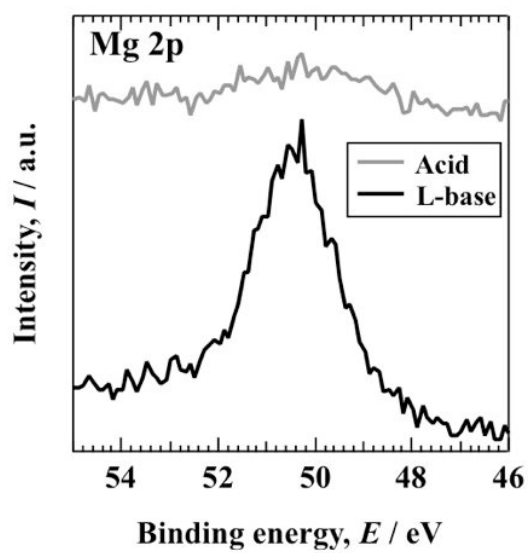
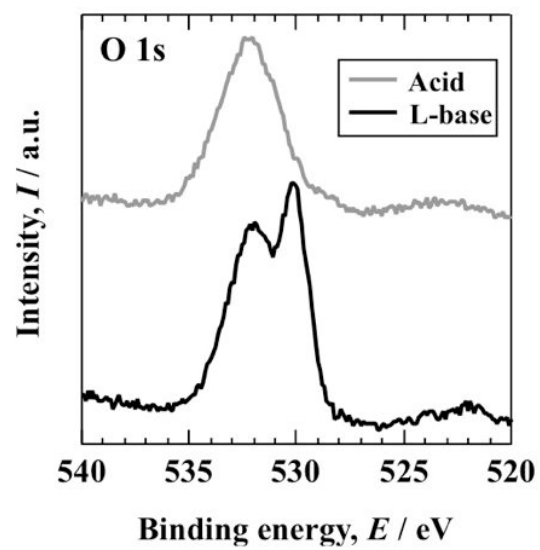
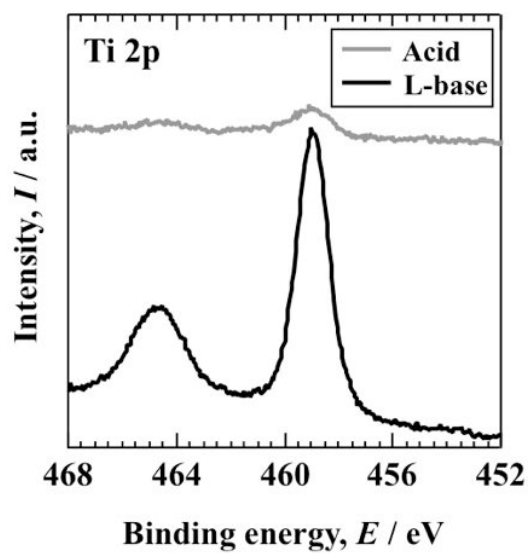


Fig. 7
R. Fujita et al.

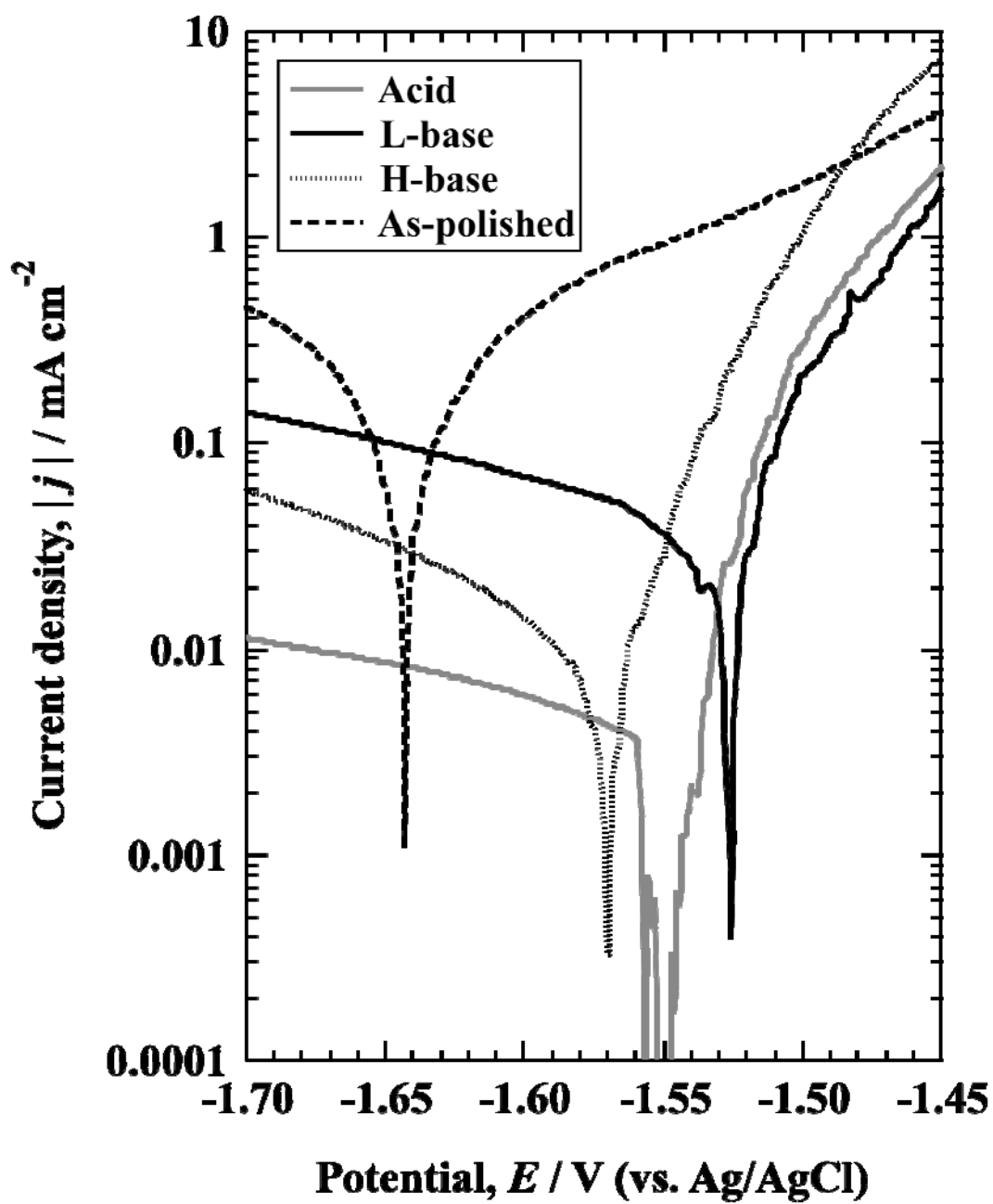


Fig. 8
R. Fujita et al.

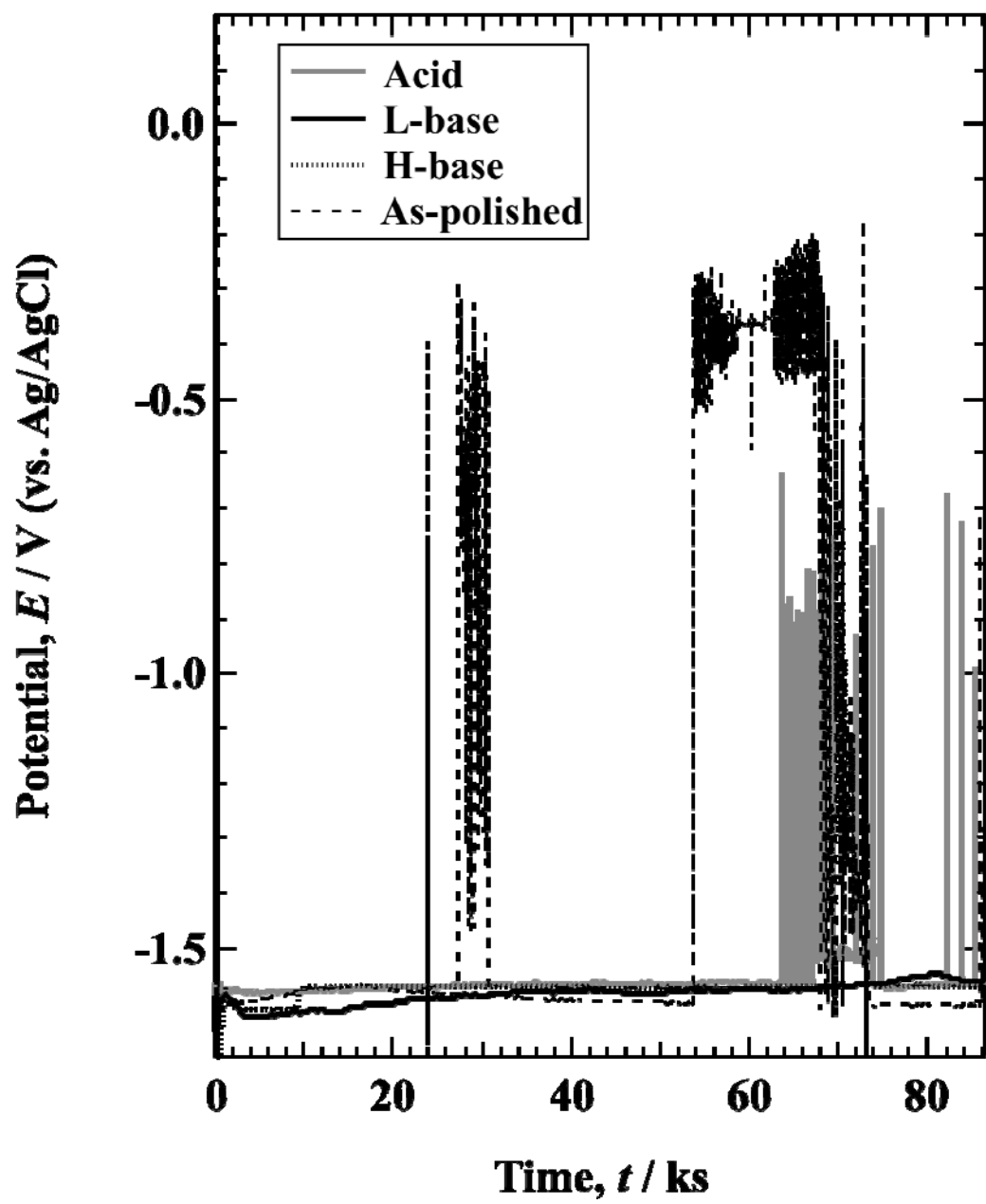


Fig. 9
R. Fujita et al.

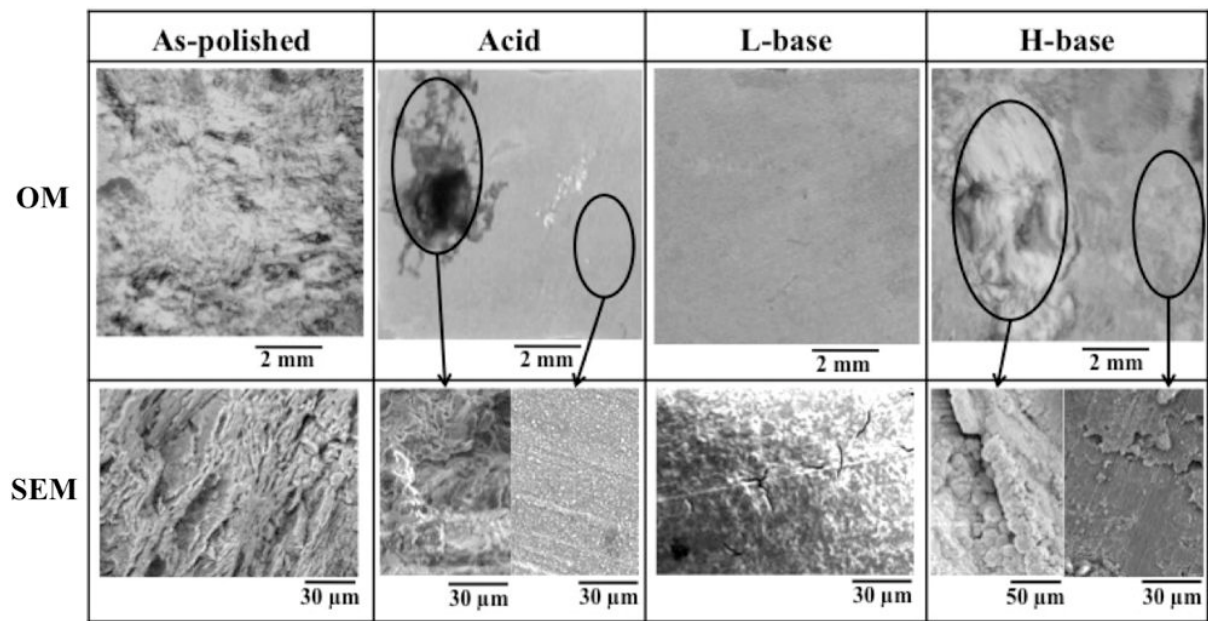


Fig. 10
R. Fujita et al.

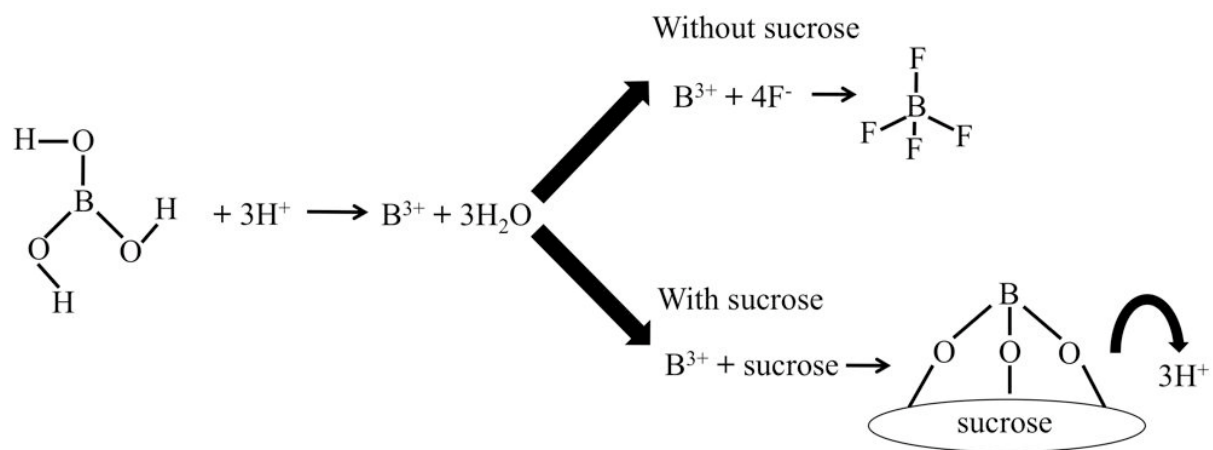


Fig. 11
R. Fujita et al.

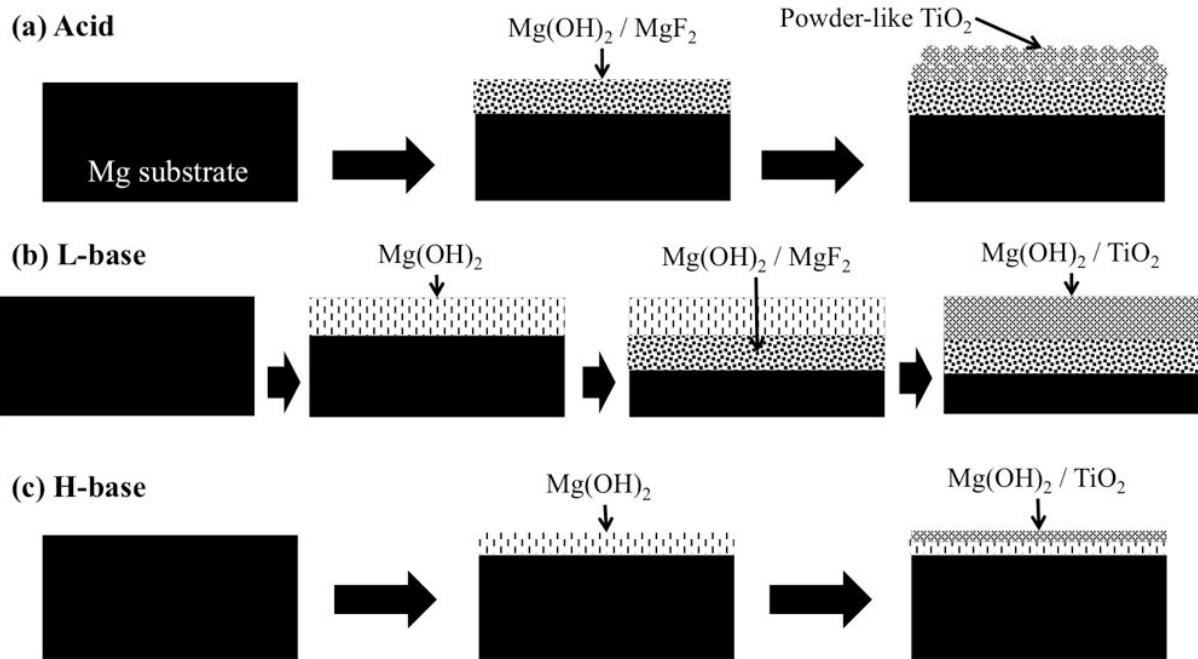


Fig. 12
R. Fujita et al.